Engineering Science and Technology, an International Journal 24 (2021) 959–973

HOSTED BY

Contents lists available at ScienceDirect

Engineering Science and Technology, an International Journal

journal homepage: www.elsevier.com/locate/jestch

Optimization of torsional vibration damper of cranktrain system using a hybrid damping approach

Haşmet Çağrı SEZGEN [a,*], Mustafa TINKIR [b]

[a] Karatay University, Vocational School of Commerce and Industry, Karatay, Konya 42020, Turkey
[b] Necmettin Erbakan University, Department of Mechanical Engineering, Meram, Konya 42090, Turkey

ARTICLE INFO

Article history:
Received 26 November 2020
Revised 13 January 2021
Accepted 8 February 2021
Available online 27 February 2021

Keywords:
Cranktrain system
Torsional vibration damper
Rubber and viscous material
Modal test and finite element method
Genetic algorithm optimization

ABSTRACT

The focus of this research is to develop the optimum design of torsional vibration damper using hybrid damping approach to decrease the torsional vibrations in the cranktrain system of internal combustion engines (ICE). For this purpose, a double mass rubber and viscous torsional vibration damper (DMRV-TVD) are combined. The optimization procedure is carried out using genetic algorithm (GA) to determine the best hybrid damping performance on cranktrain system of a four stroke and four cylinder diesel engine. Accordingly, twelve degrees of freedom lumped mass mathematical model of the proposed cranktrain system is created. The stiffness and damping coefficients of viscous and rubber materials used in DMRV-TVD model are verified by modal test and finite element natural frequency analysis. Then, the excitation torque is calculated considering the inertia forces and gas force, and Fourier series expansion is performed to obtain the harmonics of driven torque as the input load on the relevant masses. The relative angular deflection of the front end point of the crankshaft is determined. Additionally, in order to decrease the torsional vibrations of the crankshaft, DMRV-TVD model is optimized depending on the viscous material parameters by defining the boundary conditions and objective function of the genetic algorithm. The comparative results show that the developed hybrid design of optimized DMRV-TVD reduced the torsional vibrations by 50.17% when compared to the non-optimized DMRV-TVD. This achieved reduction in the torsional vibrations is expected to increase the engine performance and its durability as well as providing a better driving comfort and fuel efficiency.
© 2021 Karabuk University. Publishing services by Elsevier B.V. This is an open access article under the CC BY-NC-ND license (http://creativecommons.org/licenses/by-nc-nd/4.0/).

1. Introduction

The high speed internal combustion engines have to operate with high cylinder pressure because of the environmental, commercial and technical demands [1]. Components subject to vibration loads, such as the cranktrain, also must be optimized to increase efficiency. The cranktrain system of ICE simply contains crankshaft, flywheel and crank-pulley as torsional vibration damper (TVD). A crankshaft, which is subjected to periodic dynamic loads, must be able to withstand the torsional vibrations for a better driving comfort, fuel saving, passenger safety and durability of cranktrain system in heavy-duty internal combustion diesel engines (ICDE). The properties and compatibility of these parts have a significant impact on the torsional vibration and crankshaft fatigue-life of an ICE.

Previous research show that traditional analytical methods [2], computer aided engineering methods [3] and test methods [4] have been successfully implemented to optimize the torsional vibration damping. For example, a study conducted by Horváth and Égert [2] for a single cylinder engine reported that critical speeds were determined for the resonance phenomena that may arise from torsion natural frequencies and harmonic frequencies of excitation forces. As a result of the study, a detailed inference was obtained on resonance frequency and harmonic vibration frequencies. Cavalli et al. [3] presented dynamic calculations of a gasoline V6 engine with traditional analytical methods and AVL Excite software. They reported that the results cannot be approximated since the conditions such as hydrodynamic effects, body flexibility, real profiles of the contacting surfaces as well as deviations due to temperature were ignored in traditional methods. Janssens and Britte [4] studied the torsional vibration testing methods on four cylinder high speed diesel engine and the accuracy and performance of the proposed measurement techniques were compared. They reported that the measurement techniques such as zebra tape, incremental encoder, and dual beam laser

* Corresponding author.
E-mail address: hasmet.sezgen@karatay.edu.tr (H.Ç. SEZGEN).
Peer review under responsibility of Karabuk University.

https://doi.org/10.1016/j.jestch.2021.02.008
2215-0986/© 2021 Karabuk University. Publishing services by Elsevier B.V.
This is an open access article under the CC BY-NC-ND license (http://creativecommons.org/licenses/by-nc-nd/4.0/).

resulted in with the similar accuracy. The efficiency of the parameters can be observed and improvements can be made in dynamic models that have mass, stiffness and damping parameters, which are obtained by traditional or computer-aided methods and verified with test methods. For example, the computational model of elastomer parts were considered by Píštěk and Svída [5] to reduce the vibrations and noise when designing powertrains and automobiles. They reported that the results obtained through computational model approached the experimental results. Ni et al. [6] optimized the injection angle to minimize torsional vibrations using the lumped mass and Matlab/Simulink model of a diesel engine and the proposed models were verified with test data in their study. Silva et al. [7] considered that the effects of temperature change on the stiffness and damping of the rubber material were emphasized and the optimum range was determined for the performance of torsional vibration damper with vibration damping. Sun et al. [8] used AVL Excite Designer, CAE software and a lumped mass models to reduce the vibration of the cranktrain system and modeling results are verified with the experimental ones, and it was concluded that both methods give accurate results.

Although methods such as energy methods and transfer matrix method are used to obtain the equation of motion in traditional analytical methods, the discrete system method is mostly used. In another literature work, a new model was developed for torsional vibration damper, a viscoelastic material and a torsion spring were designed as a couple by Píštěk et al. [9]. It is difficult to design with rubber, the damping ability of which constantly changes with temperature. Therefore, in order to ignore the heat effect and not compromise the damping ability, the spring element was used and the desired performance was achieved. Sentyakov et al. [10] developed a mathematical model and algorithms for the numerical solution to the differential equations allowed us to choose the optimal parameters of the boring mandrel damping element. As a result of their study, it was found that the use of vibration damper can significantly reduce the amplitude of the boring mandrel natural vibrations when pulsed, and also significantly reduce the forced vibrations amplitude when exposed to periodic disturbing forces. Tan et al. [11] introduced the torsional vibration damper using an innovative method by combining two different parametric optimization methods; energy and modal inertia methods. It has been shown that multi-degree of freedom TVDs provide advantage in parameter optimization, but lose this advantage in low degree of freedom TVDs. Storm et al. [12] used the flexible multibody dynamics simulation to verify the results of torsional vibration models that they made harmonic analysis with Transfer Matrix Method. Also the cranktrain system was modeled using a lumped mass model, combustion pressures were obtained from the test data and precisely calculated moment of inertia was given for the excitation torque in equations of motion that was revealed to angular displacements in high resolution. Ying et al. [13] created the non-constant inertia model to observe the non-linear torsional vibrations of a crankshaft in an ICE. In another related research, Mendes et al. [14] presented the torsional vibrations of a crankshaft using two lumped mass mathematical model approaches considering a single mass viscous torsional vibration damper and a double mass rubber TVD. According to the excitation torque map, implications were made about what kind of TVD design should be chosen.

Torsional vibration dampers can be manufactured from containing rubber-dampers, viscous dampers, or both. Since the mechanical behaviors of rubber and silicone materials do not show a linear elastic, methods specific to the material models should be used in the calculation of stiffness and damping coefficients. The design criteria were determined in order to minimize torsional vibrations of the rubber bearing rotor system driven at different frequencies and, stiffness and damping coefficients were obtained for a realistic lumped mass model by Zhu et al. [15]. When modeling TVD at flexible dynamics methods, the stiffness (k) and damping (c) coefficients of the materials used must be obtained. Viscous and rubber materials, which are elements of TVD, do not exhibit a linear behavior. Talebitooti and Morovati [16] studied on dynamic calculations for these types of materials, considering their 3rd and 4th order nonlinear effects. Kim et al. [17] used test data from uniaxial and volumetric compression for calibration of the hyperelastic and hyperfoam constitutive models with the goal of simulating a compressive-loading event. They observed that a standard finite element method software was inadequate for the cranktrain, which was subjected to harmonic excitation forces due to variable mass inertia and gas pressure according to the rotational speed. Desavale and Patil [18] investigated torsional and bending effects of a cranktrain system with a simple pulley instead of a torsional vibration damper using finite element method and modal test. The results of the two different CAE software, Ansys and Hypermesh were found to be very similar. Quiroga et al. [19] calculated the torsional natural frequencies of multi-degree of freedom of cranktrain system using Holzer method and, the convergence of the results was revealed by comparing with the results of Ansys software. Sheng et al. [20] investigated rubber-type torsional vibration damper strength test and the obtained results were compared with computer aided engineering (CAE) using Mooney-Rivlin hyperelastic material model. Shahane and Pawar [21]showed that according to the result of static loading without moving away from the natural frequency values of the original model, the design is changed in the regions where the stresses are high and then the stresses are decreased.

It has been observed that the aforementioned harmonic excitation forces can be defined and even with parameters such as bearing, lubrication, friction and temperature, advanced multi-body dynamics software is better in torsional vibration calculations. Mitianiec and Buczek [22] simplified the geometry using lumped mass model to examine the torsional vibrations of a six-cylinder diesel engine in the crank system and, they obtained critical vibration cycles by Fourier analysis, taking into account firing orders. Generally valid information has been obtained about how much damping effect of TVD in which situations. Foltz et al. [23] analyzed the torsional vibrations of a high-powered diesel engine using the computer-aided multi-body dynamics method, a timing gear train was added to the model in addition to the literature. Drápal and Novotný [24] created a detailed model of the cranktrain system using Adams software and, through this model, the effect of vibration on bearing friction was observed and torsional vibrations were developed to increase the efficiency. The cranktrain system was modeled with different techniques and torsional vibrations were investigated by Armentani et al. [25]. Taking the irregularities by the engine orders into consideration, the realities of the models were compared in this research. In another study, optimization parameters were obtained by comparing different methods for a new design to be more durable by minimizing torsional vibrations in the cranktrain system by Karimaei et al. [26].

In the relevant literature surveys outlined above, different theoretical models, finite element models, experimental and test studies on cranktrain systems were realized and very important findings have been obtained. According to these studies, it was observed that the cranktrain system was examined by considering one or more elements of torsional vibration damper, crankshaft, connecting rods, and flywheel. The researchers also focused on TVD to decrease the torsional vibrations occurring in the crankshaft. The torsional vibration is of great importance for the cranktrain system especially in diesel engines with high speed. Different type of pulleys such as double mass rubber torsional vibration damper (DMR-TVD) and viscoelastic torsional vibration damper

(V-TVD), were considered and investigated in literature according to the type of internal combustion engine. The dampers used to absorb the torsional vibration are generally designed using rubber or viscous dampers for high torque and high horsepower engines. Wakabayashi et al. [27] preferred rubber material as a damping element in TVD models. They compared the torsional vibrations in the crankshaft as 3 models, without TVD, A-type rubber TVD, B-type rubber TVD. Although they did not mention the performance of the B-type rubber damper, they reduced torsional vibrations by approximately 35%. A rubber material design has been considered by Ramdasi and Marathe [28] to absorb the high amplitudes that occur in the torsion axis during resonance considering the different harmonic orders. According to the results, the torsional vibrations are reduced by approximately 50% with TVD. Villalva at al. [29] considered the harmonic vibrations, a rubber-type TVD is optimized through AVL software, and the effect of optimization on the stress state caused by torsional vibrations is observed. For comparison, no damper, untuned, tuned unitary and tuned optimum cases are considered and the stress is reduced by approximately 25%. Píštěk et al. [30] reported that rubber damper was not sufficient as harmonic vibration damping element for heavy duty diesel engines, and they designed an unconventional rubber torsional damper with two degrees of freedom to optimize the parameters. Their results showed that the twin rubber damper was approximately 50% better in torque transmission when compared to the rubber damper. Kodama and Honda [31] considered a torsional vibration damper containing only silicone oil as a damping element and the dynamic characteristics of this product were compared with the discrete system model and experimental results. They reported that silicone oil was very effective as a damping element and the validity of the damping and stiffness coefficients was proven by verifying the split system model with test results.

Although a reduction in the torsional vibration was achieved to some extent as referenced above, these studies were conducted by design of experiments and not based on an optimization through a mathematical model. Thus, new and novel approaches are necessary to design and optimize dampers for the required damping capability. Various approaches have been investigated on the torsional vibrations of the cranktrain system by many researches in literature, however as in this study, a novel design double mass rubber viscous torsional vibration damper (DMRV-TVD) has not been addressed and genetic algorithm (GA) based optimization of proposed system has not been handled. Motivated by this fact, the main contribution and objective of this paper are described as follows:

i. A novel design and optimized double mass rubber and viscous torsional vibration damper (DMRV-TVD) are developed to suppress the torsional vibrations of the cranktrain system.
ii. Genetic algorithm-based TVD optimization is carried out for the first time both in scientific and industrial terms.
iii. Twelve degrees of freedom of a novel lumped mass mathematical model consist of the DMRV-TVD is formed and verified by natural frequency analysis using modal test and finite element method.
iv. Approaches used to determine the stiffness and damping coefficients of the verified modeling can be employed for any multi degree of freedom vibration systems.

2. The dynamic modeling of the cranktrain system

Although many computer-aided engineering softwares are used in the studies on the modeling of the cranktrain system, all of them are based on a theoretical model [32–34]. Therefore, in this paper, the theoretical model that will give the most realistic results is proposed and, the equations of the motion of twelve degrees of freedom of a lumped mass mathematical model are considered. TVD is the important part of the cranktrain that damps the harmonic vibrations and, it consists of different mass and damping components. However, in the dynamic modeling approach, a double mass rubber and viscous torsional vibration damper (DMRV-TVD) are used with two different damping elements; rubber and a viscous material. Such design is considered in this study because different damping elements are needed to absorb loads with different dynamic characteristics.

The cranktrain system has a highly detailed and complex dynamics. Hence, below remarks should be considered when dealing with the torsional vibration and its optimization.

1. Excitation torque caused by gas pressure and inertia forces differs in each rotation and has different firing sequences depending on the number of cylinders. This is a phenomenon defined as harmonic order and causes different natural circular frequencies to be forced in each cycle. Therefore, when defining the cylinder forces for each rotation, the excitation torques expanded with Fourier series should be calculated.
2. The stiffness and damping coefficients of the viscous silicon fluid and rubber materials in the torsional vibration damper are non-linear. Therefore, it is necessary to create a specific model for the mechanical behavior of these materials.
3. It is very difficult to calculate the torsional vibration when the parts in the system are considered as a continuous structure. Therefore, the system is simplified and the lumped mass model expressed by a finite number of masses, springs and dampers are established.

2.1. Torsional lumped mass model

In the literature, different lumped mass models including various TVD models have been used to obtain the dynamic modeling of the cranktrain system and natural frequencies [28,35]. However, in this study, a novel torsional lumped mass model of the cranktrain system using DMRV-TVD is developed as given in Fig. 1 and the equations of the motion are obtained to simulate the elative angular deflections and relative angular velocities. The calculated natural frequencies verified based on the reported modal test and FEA [36].

Torsional lumped mass model has twelve degrees of freedom and consists of three main parts as flywheel, crankshaft and DMRV-TVD. In the model given in Fig. 1, two inertia masses (J_1 and J_2) for the flywheel, five inertia masses (J_3, J_4, J_5, J_6 and J_7) for the rods and front end of the crankshaft, and five inertia masses (J_8, J_9, J_{10}, J_{11} and J_{12}) for DMRV-TVD are adopted. In the novel design of the DMRV-TVD, the assembly hub (J_8) is connected to the inner hub (J_9), body mass (J_{11}), inertia mass (J_{12}) with springs and dampers. The inner hub (J_9) is also related to a pulley (J_{10}) with spring and damper. The rubber material is defined as k_9 and c_9 and, viscous silicone fluid is assigned to k_{11} and c_{11} in lumped mass model of the DMRV-TVD. The rubber is between the inner hub (J_9) and the pulley (J_{10}) and, it ensures that the pulley (J_{10}) rotates with a certain phase angle with the crankshaft for damping harmonic orders of the torsional vibrations. Moreover, the inertia mass (J_{12}) is replaced into the body mass (J_{11}) and, viscous silicone fluid is filled in the clearance between these two masses. This viscous fluid allows rotation of the inertia mass (J_{12}) in the body mass with a certain phase angle with the crankshaft. Thus, the sub-harmonic orders of the torsional vibrations of the crankshaft are damped via this phenomenon. Therefore, in this study, this novel DMRV-TVD model is created to decrease the torsional vibration irregularity in cranktrain system. The equations of the motion of the proposed lumped mass model are given below.

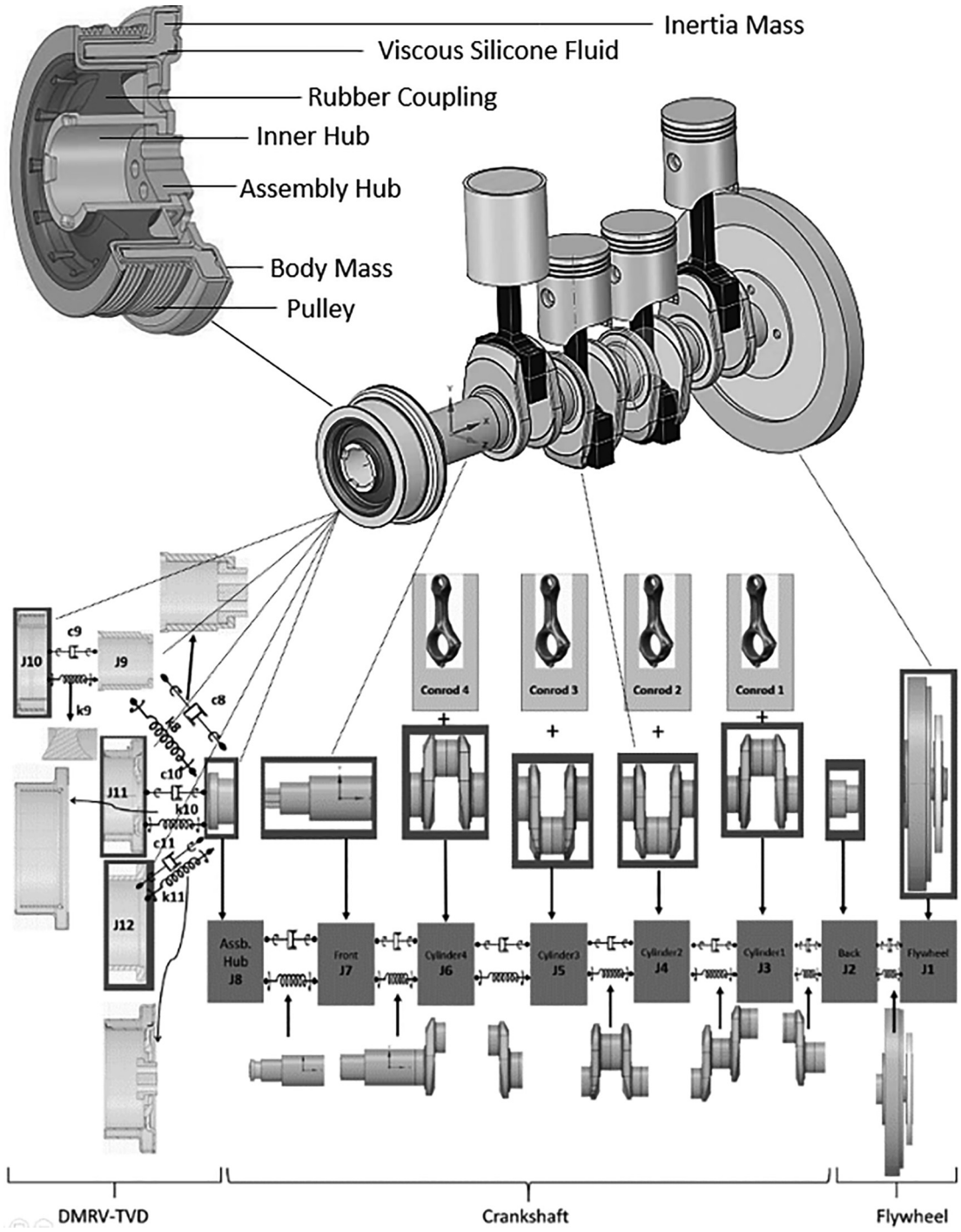

Fig 1. Torsional lumped mass model of the cranktrain system using DMRV-TVD.

$$[\boldsymbol{J}]\left\{\ddot{\theta}(t)\right\} + [\boldsymbol{C}]\left\{\dot{\theta}(t)\right\} + [\boldsymbol{K}]\{\theta(t)\} = T(t) \quad (1)$$

The equations of the motion are presented as state-space model in Eq. (2) where X is state variables, U is inputs, Y is outputs, A,B,C and D are state matrixes. The extended state space model is given in the Appendix 1.

$$\dot{\boldsymbol{X}} = A\boldsymbol{X} + B\boldsymbol{U} \text{ and } \boldsymbol{Y} = C\boldsymbol{X} + D\boldsymbol{U} \quad (2)$$

2.2. Inertias, torsional stiffness and damping coefficients

2.2.1. Crankshaft and flywheel

The lumped mass model of a four-stroke four-cylinder diesel engine is considered using twelve mass moments of inertia corresponding to twelve masses in the proposed model. Three dimensional solid model of a four-stroke four-cylinder diesel engine is used to calculate the mass moments of inertia in the rotation

direction. These masses are connected to one another by torsional stiffnesses and torsional damping. The B.I.C.E.R.A. formulation [37] and finite element approach are utilized to obtain the torsional stiffness of the masses of the crankshaft and flywheel. Each stiffness part of the crankshaft and flywheel shown in Fig. 2, torque is applied from one side while the other side is kept constant.

Torsional stiffness coefficients (k_t) aZre calculated based on Eq. (3), which gives the relationship between torque (T) and the calculated torsion angle (θ).

$$T = \boldsymbol{k_t}\theta \tag{3}$$

The relative damping coefficient (c_r) of the crankshaft and flywheel can be obtained by the loss factor calculation as given in Eq. (4):

$$d = \frac{\boldsymbol{c_r}\omega_n}{k_t} \tag{4}$$

where d is the loss factor according to [38,39], ω_n is the natural frequency (rad/s) of the crankshaft and flywheel, c_r is relative damping ratio. Absolute damping ratio of the crankshaft and flywheel is reached by the contact between the piston rings and the block with oil films depending on the crankshaft position.

2.2.2. Rubber and viscous material

In order to determine the stiffness coefficient of the rubber ($k_{trubber}$) material used in DMRV-TVD, Eq. (5) is written as follow:

$$T = \boldsymbol{k_{trubber}}\theta = \frac{\pi G_r D_o^4 - D_i^4}{32l}\theta \tag{5}$$

where G_r is shear modulus, D_o and D_i are inner and outer radius of the rubber, respectively, and l is the length. The rubber geometry of the DMRV-TVD is given in Fig. 3.The rubber tensile test shown in Fig. 4 is realized to determine G_r as given in Eq. (5) and, average G_r value is calculated between minimum and maximum excitation torques according to the test results. Moreover, the test results are used in FEA to verify the Eq. (5).

Since the stress–strain test output is non-linear, it is necessary to select a material model suitable for the curve in order to use it in a mathematical model. Mooney-Rivlin is chosen as the most suitable material model for the obtained curve. The curve-fitting is made using Mcalibration software to obtain Mooney-Rivlin coefficients [40]. As can be seen in the figure, curves diverge in large strain values. If the nine-parameter Mooney-Rivlin is used, curves will also converge on large strains. The highest strain value obtained with the five-parameter Mooney-Rivlin will be sufficient for the strain to occur in this study. The material properties are

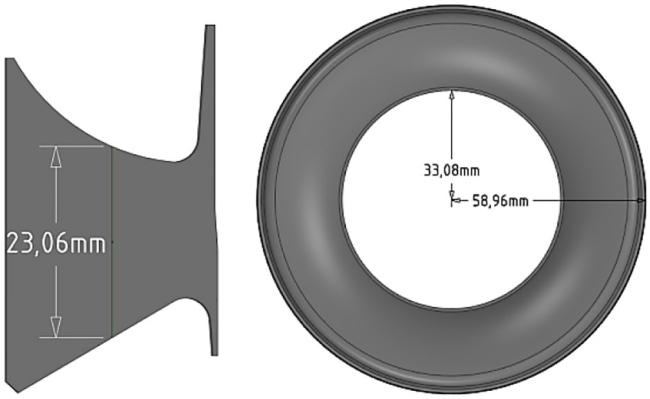

Fig 3. The rubber geometry of the DMRV-TVD.

defined in FEA, the process applied to the other elements is repeated and stiffness is obtained using Eq. (5).

The torsional stiffness of viscous material is given in Eq. (6) which gives the dynamic torsional stiffness as a function of kinematic viscosity.

$$k_{tviscous} = G_k e^{B_k/T} n j^{a_k - \frac{a_{k1}}{T}} S \tag{6}$$

where T is absolute mean temperature of the silicone film (K), n is engine speed (s^{-1}), j is order number and S is described as clearance factor (m^3).

Eq. (6) and G_k, B_k, a_k, a_{k1} constant parameters are obtained from the performed tests using different viscous fluids at different temperatures and excitation frequencies [14,38]. For the relative damping coefficient of the rubber material, the loss factor is selected in the range of $0.15 < d < 0.25$ and calculated according to Eq. (4).

The relative damping coefficient of the viscous fluid in the torsional vibration damper is calculated by Eq. (7).

$$c_{tviscous} = \frac{G_c e^{\frac{B_c}{T}} n^{a_c - \frac{a_{c1}}{T}} S}{2\pi n j} \tag{7}$$

where G_c, B_c, a_c, a_{c1} are the material constants. These constants and the stiffness coefficient of the viscous material are obtained empirically from the same test set up. The constants of the viscous material are given in the Appendix 2.

2.3. Matrix method: undamped free vibrations of the DMRV-TVD

Total external torque (T_T) applied to DMRV-TVD is defined as:

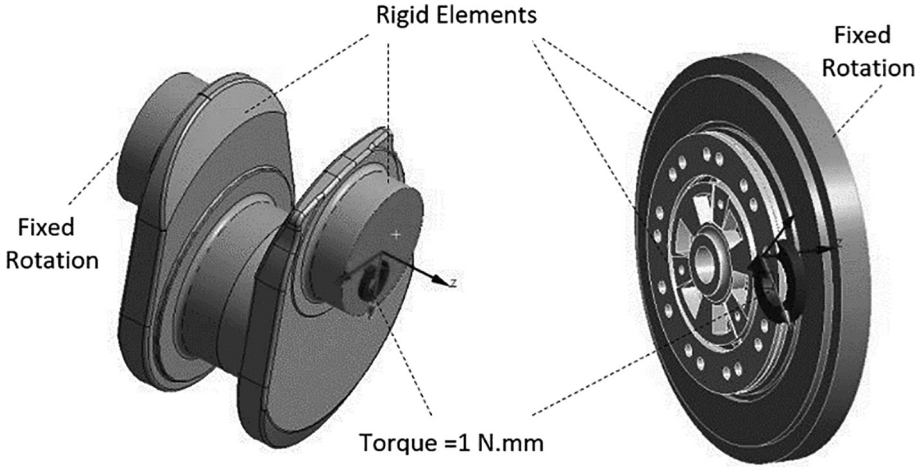

Fig 2. The torsional stiffness of the crankshaft and flywheel using FEA.

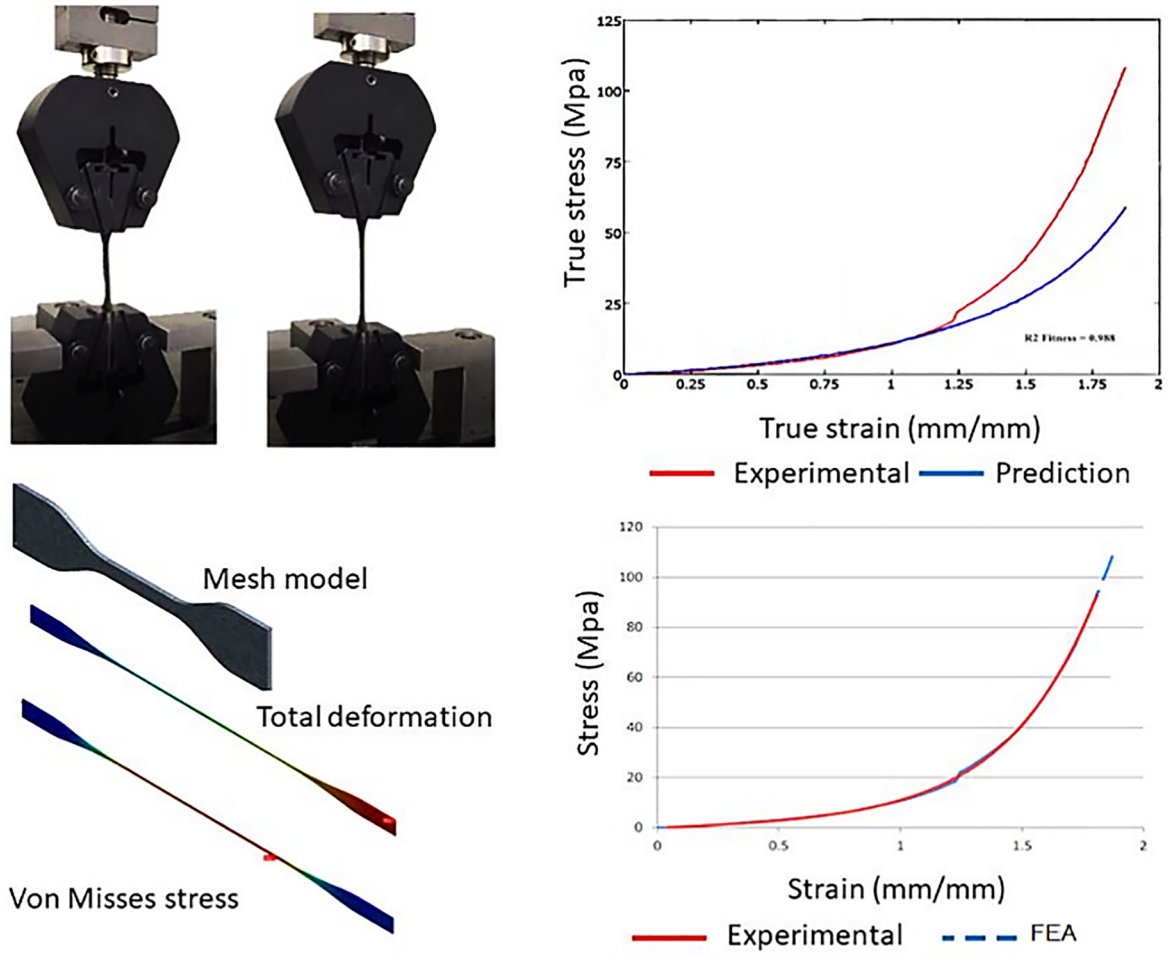

Fig 4. The rubber tensile test and FEA verification.

$$T_T = J_n \ddot{\theta}_n \tag{8}$$

The simple harmonic motion of a rotational body is described as:

$$\theta_n(t) = \theta_n \sin\omega_{nf} t; \ddot{\theta}_n = -\omega_{nf}^2 \theta_n \sin\omega_{nf} t = -\omega_{nf}^2 \theta_n \tag{9}$$

where θ_n is torsional vibration amplitude, J_n is polar moments of inertia and ω_n is torsional natural frequency of the DMRV-TVD. The equation of motion of DMRV-TVD in the lumped mass model is written in matrix form as follows.

$$\left\{ -\omega^2 n_f \begin{bmatrix} J_8 & 0 & 0 & 0 & 0 \\ 0 & J_9 & 0 & 0 & 0 \\ 0 & 0 & J_{10} & 0 & 0 \\ 0 & 0 & 0 & J_{11} & 0 \\ 0 & 0 & 0 & 0 & J_{12} \end{bmatrix} + \begin{bmatrix} k_8+k_9+k_{11} & k_8 & 0 & -k_{10} & -k_{11} \\ -k_8 & k_8+k_9 & -k_9 & 0 & 0 \\ 0 & -k_9 & k_9 & 0 & 0 \\ -k_{10} & 0 & 0 & k_{10} & 0 \\ -k_{11} & 0 & 0 & 0 & k_{11} \end{bmatrix} \right\} \begin{bmatrix} \theta_8 \\ \theta_9 \\ \theta_{10} \\ \theta_{11} \\ \theta_{12} \end{bmatrix} = \begin{bmatrix} 0 \\ 0 \\ 0 \\ 0 \\ 0 \end{bmatrix} \tag{10}$$

The matrix form is similar to bending vibration; the difference of which is that polar moments of inertia and torsional stiffness are used instead of mass and bending stiffness, respectively. According to Eqs. (10), Eq. (11) can be written as the eigenvalue problem solving approach.

$$-\omega_{nf}^2 [M] + [K]\{\theta\} = \{0\} \tag{11}$$

$$[\lambda] = [M]^{-1}[K] \tag{12}$$

here the eigenvalue is described as λ and, the torsional natural frequencies are calculated according to Eq. (12) and it is given in Eq. (13).

$$\omega_n = \begin{bmatrix} 3.116.10^4 \\ 5.797.10^3 \\ 321.413 \\ 25.091 \\ 3.723.10^{-5} \end{bmatrix} = \begin{bmatrix} \text{4th torsional natural frequency} \\ \text{3rd torsional natural frequency} \\ \text{2nd torsional natural frequency} \\ \text{1st torsional natural frequency} \\ \text{Rigid body mode} \end{bmatrix} \tag{13}$$

Also the eigenvector V is found as follow:

$$V = \begin{bmatrix} 0.998 & -0.339 & 0.513 & 0.252 & -0.447 \\ -0.057 & -0.94 & 0.514 & 0.252 & -0.447 \\ 2.868.10^{-8} & 1.362.10^{-5} & -0.002 & -0.862 & -0.447 \\ -0.004 & 0.045 & 0.527 & 0.252 & -0.447 \\ -4.903.10^{-5} & 4.823.10^{-4} & -0.44 & 0.256 & -0.447 \end{bmatrix} \tag{14}$$

2.4. Modal test and finite element natural frequency analysis

Linear elastic material properties are used for steel and plastic parts in the model. However, for rubber and silicone parts, more extensive material properties must be used. Therefore, the necessary mechanical tests have been carried out to obtain the material properties of these parts for the finite element model. For this purpose, the modal test and finite element modal analysis of DMRV-TVD are realized and given in Fig. 5.

Ansys modal module is used to obtain the natural frequencies and mode shapes of DMRV-TVD. Surface simplifications are made

via Spaceclaim software in order to obtain a more suitable mesh model for the DMRV-TVD, which is computer aided design (CAD) in accordance with the reality. The geometry is transferred to the modal module and the contact definitions, the creation of the mesh model and the boundary conditions are provided to obtain the mode frequencies and shapes. A total of 25 contacts are used for the finite element model (FEM) of the DMRV-TVD which consists of 14 assembled parts. 20 of the contacts are connected with bonded contact (faces cannot be separated from each other) and 5 of the contacts are connected by frictional contact (they can slide on each other and the faces can be separated from each other). Body mass, inner hub, teflon bearing and 3 plastic washers are connected with frictional contact. While creating the mesh model, the number of nodes is increased in the contact surface resulting in more sensitive meshes, especially in frictional contact areas. Although Hex20 elements are mostly used, for the parts with high curvature, Tet10 elements are used by defining the element size parametrically, the optimum element size is determined at the point where the element size - frequency graph is fixed. In the FEM model of the DMRV-TVD, the rotation axis is freed as in the lumped mass model. By considering the first 2 modes, mode shapes and mode frequencies outputs are obtained.

While in the actual situation the crankshaft is fixed to the hub, for the DMRV-TVD modal test, a shaft is fixed to the hub. The accelerometer is connected to the pulley part, which is the outer part of the DMRV-TVD. On the same part, a part is attached to the opposite side of the accelerometer to hit it with a modal hammer. The responses of the pulley excited by the modal hammer on the rotary axis are collected from the accelerometer. By connecting the accelerometer and modal hammer to the Dewesoft device, the productive sensitivity values of the accelerometer are entered. After opening the modal test interface with the DewesoftX software, the accelerometer and modal hammer force data are checked. During the test, it is important to operate with a single touch and avoid a double hit from the hammer. After the force from the hammer and the acceleration data from the accelerometer are recorded, the modal frequencies are checked from the FFT Graph. The accuracy of the peaking values is also compared with the data obtained in the modal analysis. If harmonic frequency is suspected, stabilization control can be done with LMS software. The rubber material exhibits mechanically hyperelastic behavior, thus, the Mooney-Rivlin model is used. The necessary inputs for this model are obtained by processing the tensile test results with Mcalibration software [40]. After verification of the modal test and FEA for the rubber material, the Mooney-Rivlin model is performed for DMRV-TVD. The obtained torsional natural frequency results are given in Fig. 6 and they are explained in Table 1.

The modal test results of the considered DMRV-TVD model are accepted as reference values for the results found with other methods. While preparing the lumped mass model, the stiffness coefficients of rubber and silicon oil material are calculated depending on the excitation frequency and harmonic order value. The excitation frequency and harmonic order are taken according to the situation where the most critical torsional vibrations will occur. Therefore, while the first mode at low frequency is not close to the reference value, the frequency values in the solution of the second mode with lumped mass and FEA have been found satisfactory.

3. The calculation of the excitation torques

The excitation torque acting on the cranktrain system consists of pressure caused by the combustion gas torque in the cylinders, the inertia torque of the connecting rod and the piston, the braking torque, the torque from the connecting gears, the pulley and the flywheel. The oil pump, gas pump, air conditioning motor, valve train, fuel pump, transmission and other accessories are driven by the torque transmitted from the pulley and flywheel. Usually only the combustion gas torque and reciprocating inertia torque are taken into account and accessories are ignored since their torque is low. When a cylinder is considered, torque is calculated by multiplying the sum of tangential cylinder pressure force and tangential inertia force by the crank Radius. Only tangential forces are taken into account since the torsional vibration analysis is calculated. In order to obtain the tangential cylinder pressure force, it is necessary to obtain the cylinder combustion pressure curve specific to the related engine and to know the geometric properties of the piston. The tangential force (F_T) transmitted to the connecting rod by the cylinder combustion pressure and the reciprocating mass is given as follow:

$$F_T = (F_p + F_i) \cdot \frac{\sin(\theta + \beta)}{\cos\beta} \tag{15}$$

$$\lambda \cdot \sin\beta = r \cdot \sin\theta \tag{16}$$

In Eq. (15), F_p is the gas pressure force, F_i is the inertia force caused by the acceleration of the piston and connecting rod. Connecting rod angles (θ) depending on the crankshaft angle (β) are needed to derive the equations of motion and λ is the connecting rod length and r is the crank radius. These parameters can be obtained from the kinematic relationships of the piston-connecting rod-crank mechanism given as follow:

$$F_p = \frac{\pi \cdot D^2}{4} \cdot P(\theta) \tag{17}$$

$$F_i = (m_{p+} m_{1+} \frac{b}{l} m_3) \cdot \frac{a_p^n}{100} \tag{18}$$

where P(θ) is the pressure inside the cylinder and D is the bore diameter of the cylinder. $m_p$is piston mass, $m_1$andm_3 masses transferred from connecting rod to piston. The m_3 mass is included in the

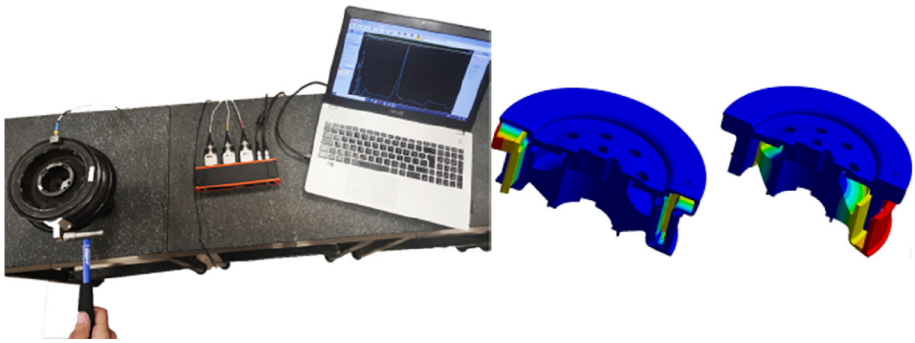

Fig 5. The modal test and FE modal analysis of DMRV-TVD.

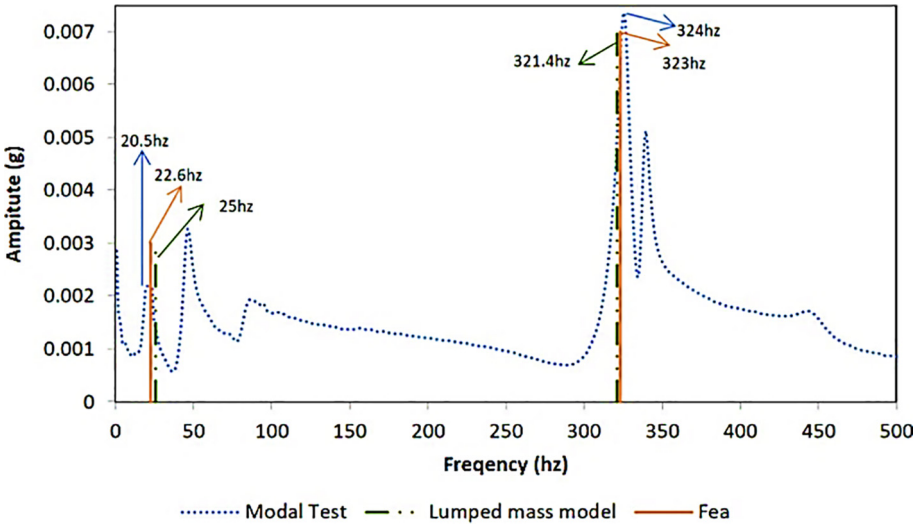

Fig 6. The results of the torsional natural frequencies using modal test, lumped mass model and FEA.

Table 1
The comparison of the torsional natural frequency results.

Method	1st torsional natural frequency	Converge %	2nd torsional natural frequency	Converge %
Modal Test	20.51	–	324	–
Lumped Mass Model	25.091	80%	321.413	92%
FEA	22.64	90.6%	323	97%

piston mass by multiplying the ratio $(\frac{b}{l})$ obtained by dividing the distance between the connecting rod center of gravity and the crankshaft by the total length of the connecting rod. a_p is the piston acceleration and n is the order number. The tangential total inertia force (F_i) and first–second order inertia forces (F_{i1} and F_{i2}) are given in Fig. 7. Also tangential combustion force (F_p) and tangential total force (F_T) are shown in Fig. 8.

The combustion force of the diesel engine considered in this study given in Fig. 8 is plotted with a pressure - crank angle graph with a maximum instantaneous pressure of 150 bar. Position, velocity and acceleration graphs are obtained depending on the geometric properties of the diesel engine and the rotational speed. Tangential total inertia force is obtained from the 1st and 2nd order acceleration versus crank angle graphs shown in Fig. 7 for the determined working speed of the engine. Tangential total force is obtained from the sum of these two curves. The periodic torque curve obtained consists of an infinite number of torsional vibrations. The torque-crank angle function can be mathematically expanded with Fourier-Transformation as harmonic series. Accordingly, the torque - crank angle function can be written using $M(\alpha)$.

$$M(\alpha) = M_m + 2\sum_{n=1}^{\infty} a_n \cos\left(\frac{2\pi}{T} n\alpha\right) + 2\sum_{n=1}^{\infty} b_n \sin\left(\frac{2\pi}{T} n\alpha\right) \quad (19)$$

here M_m is the average torque, the coefficients a_n and b_n can be calculated by the following equations:

$$a_n = \frac{1}{T}\int_0^T M(\alpha)\cos\left(\frac{2\pi}{T} n\alpha\right) d\alpha \quad (20)$$

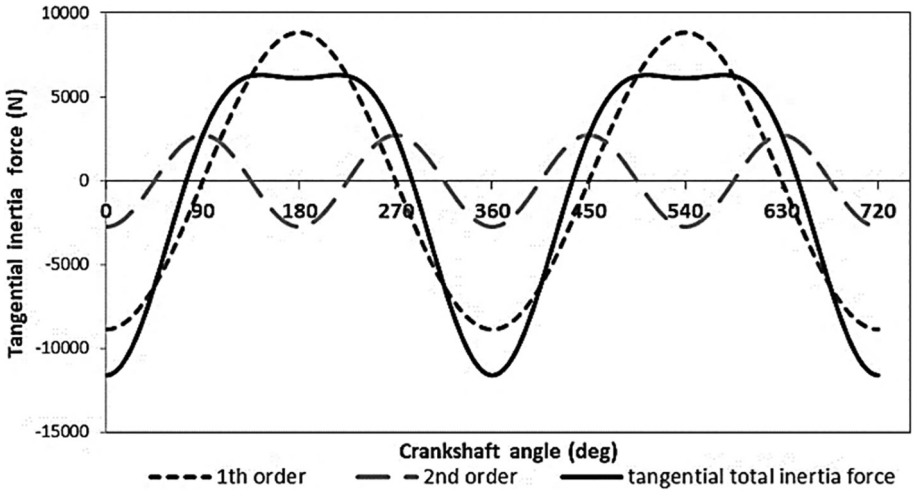

Fig 7. Tangential 1th (F_{i1}) and 2nd order inertia forces (F_{i2}) and tangential total inertia force (F_i).

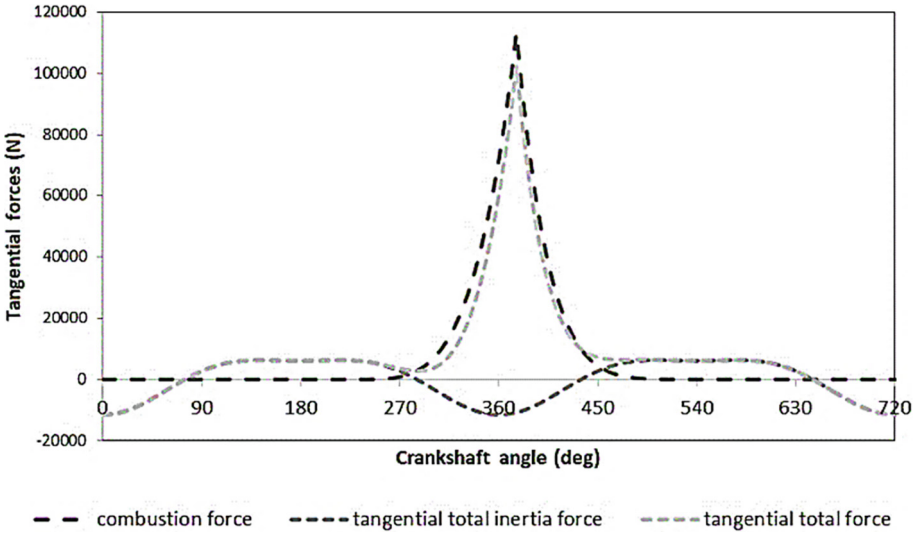

Fig 8. Tangential inertia force (F_i), tangential combustion force (F_p) and tangential total force (F_T).

$$b_n = \frac{1}{T}\int_0^T M(\alpha)\sin\left(\frac{2\pi}{T}n\alpha\right)d\alpha \tag{21}$$

In the dynamic calculations of four-stroke engines, the equation $T = 4\pi$ is used as the engine cycle period. This period value is substituted in the Eqs. (20) and (21) to obtained $\frac{n}{2}\alpha$ as the argument of the sin and cos functions. The $\frac{n}{2}$ value obtained is the n^{th} order of a series of harmonic oscillations in the all motor cycle. The harmonics will have half orders when using a four-stroke engine as in the case of $n = 1,2,3$ and $x = 0,5,1,1,5$ oscillation in the harmonic functions are given [41]. The torques of four cylinders and total torque are given in Figs. 9 and 10, respectively.

Torque - crank angle graph of 4 cylinders considered according to the firing order is shown in Fig. 9. This graph is similar to the torque graph of a typical internal combustion engine and has 4 peaks due to gas forces, while other amplitudes are due to inertia forces. In Fig. 10, the torque graphs of 4 cylinders are collected. In this graph, the torque amplitudes of harmonic frequencies are roughly seen.

4. The optimization of the DMRV-TVD

Genetic algorithm (GA) based optimization is used to find the approximate solutions for minimizing the torsional vibrations of the cranktrain systems. Also the main purpose of the optimization is to optimize the silicone fluid used as viscous material of the DMRV-TVD. The flowchart of the proposed GA based optimization is given in Fig. 11. According to the given flowchart, it is started with a population consisting of randomly generated individuals (chromosomes) represented by 0 s and 1 s. The solutions of the previous population are used to produce a new population. In each generation (iteration), the fitness of each chromosome is evaluated according to the objective function of the optimization problem and the natural selection process is realized according to these fitness values. After selection, the crossover and mutation processes are applied to the population. The crossover process creates a new generation with selected chromosomes while the mutation process changes a small fraction of the bits in the chromosomes. The new generation of the candidate solutions is then used in the next generation of the algorithm. It is expected that the newly created population is better than the current population since fit better chromosomes are selected. This process is repeated until the appropriate solution or maximum iteration number is reached. The population size, crossover and mutation rates given as inputs are the critical parameters affecting the performance of algorithm [42].

Silicone fluid material and amount of this fluid are defined as optimization variables. It is adopted that silicone fluid viscosity

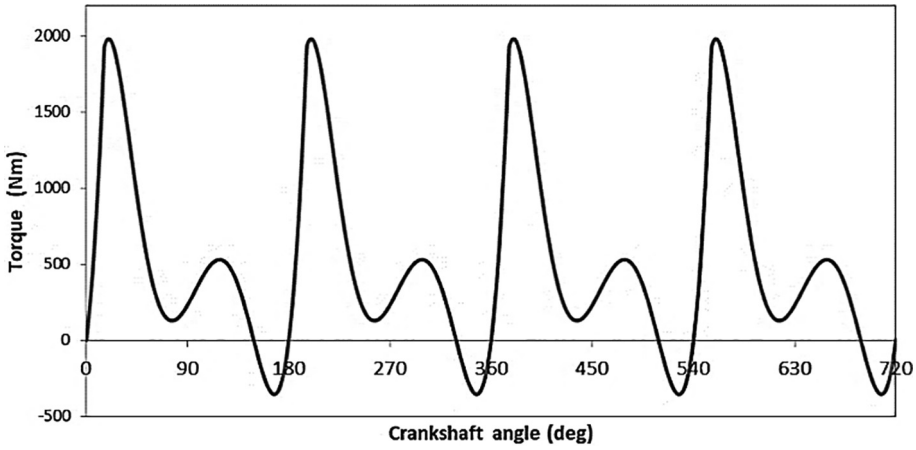

Fig 9. The torques of the four cylinders according to the firing order.

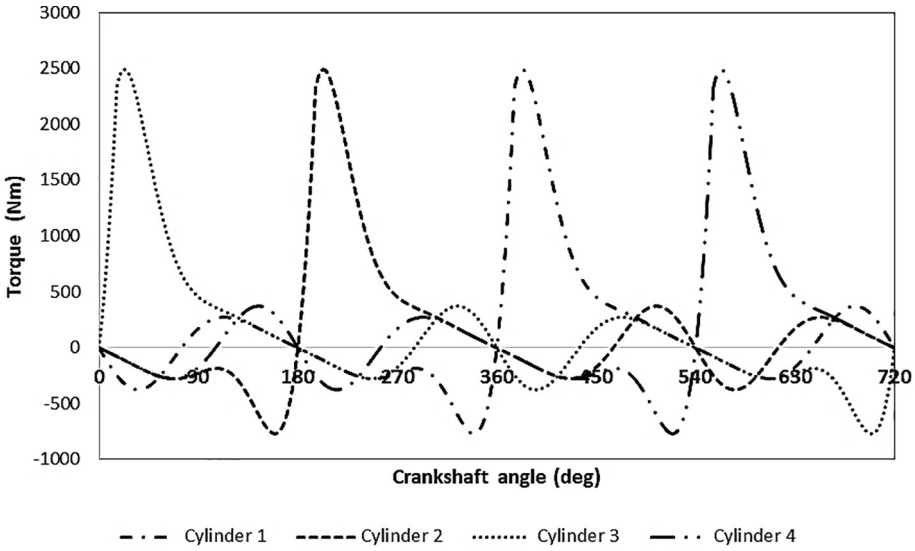

Fig 10. The total torque of harmonic frequencies of the four cylinders.

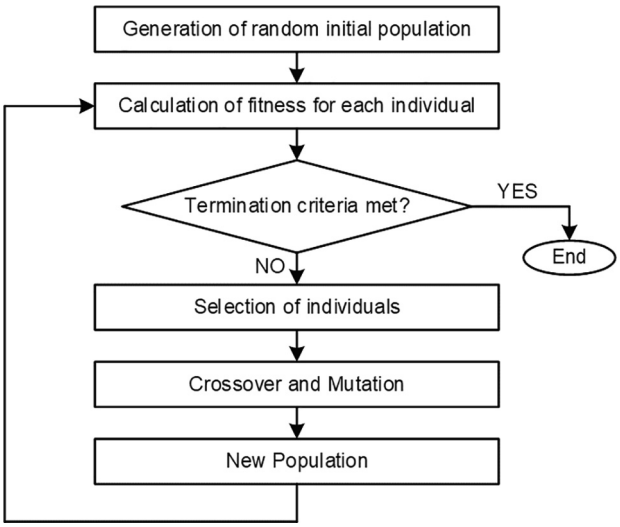

Fig 11. The flowchart of the genetic algorithm based optimization.

and the clearance factor (S) vary between 0.1–1 m^2/s and 2–10 m^3, respectively. In GA based optimization, Eqs. (6) and (7), which give the stiffness and damping coefficients of silicone fluid, are taken as two separate objective functions and they are optimized. The GA parameters and values used in this study are as follows: Population size is 50, elite count is 10 and crossover fraction is 0.6. Also the convergence performance of the proposed GA optimization is given in Fig. 12. Best fitness means the lowest fitness function among all members in the population. Mean fitness is described as the average over all members in the current population. As seen from the Fig. 12, they converged at the end of 50 iterations.

5. Results and discussion

All nodes in the cranktrain system should be considered individually when designing and optimizing the torsional vibration dampers. In this study, the system is divided into twelve masses using the lumped mass model yielding twelve nodes. While it is necessary to consider the differences in torsional angle and torsional velocity at each node, the nodes at the end points should also be examined in detail for two reasons. First of all, the end-points can be measured with test methods making the comparison of the results possible with other methods. Second, the transmission of torque at the endpoint at which the torsional vibration values should be measured more carefully. In order to accurately measure the torsional vibrations, a mathematical model must be first developed to simulate the cranktrain system in accordance with the actual values. Next, the excitation torque has to be obtained in time and harmonic order. Then, the boundary conditions should be determined and the torsional vibration data should be collected from the appropriate nodes once the system is driven.

The cranktrain system discussed in this study is expressed with a new and novel mathematical model using the lumped mass method. The excitation torque in an internal combustion engine consists of mass inertia and gas forces known to be periodic. The excitation torque is expressed as the sum of harmonic rows expanded with Fourier series, adhering to the combustion sequence specific to the engine. While the system is modeled so that the masses can rotate only in torsional axes, a single degree of freedom is defined for the nodes. In addition, excitation torque is given from four crank shaft connected to the cylinders, the other nodes are released. The rotation angles of twelve masses in one crank tour and the angular velocities are given in Figs. 13 and 14, respectively. The torsional differences of the masses are seen clearly in Fig. 14.

In order for the DMRV-TVD to be a function as a power transmission element, it must be able to damp the vibrating motion from the crankshaft transmitting to the oil pump, air conditioning engine, fuel pump and other equipment which is provided by means of belt - pulley (J_{10}). The pulley is delayed as the rotation angle and the rotation velocity as seen in Figs. 13 and 14, respectively, and therefore the incoming power is transmitted by damping. Another task of the DMRV-TVD is to damp the vibrations that occur in the crankshaft. The crankshaft end to which the DMRV-TVD is connected on the left side of the cranktrain system is expressed as J_7 in the equation of the motion in the lumped mass model. The first mass attached to the DMRV-TVD on the crankshaft side is the J_7 mass and it is seen in Fig. 14 how J_7 exhibits a damping characteristic with a delay. Due to the importance of J_7 as mentioned above, optimization studies are conducted based on the node given in Fig. 1. Fig. 15 describes the torsional vibrations at the crankshaft end (J_7) resulting from the excitation torque obtained in the sum of 16 harmonic orders at 2100 rpm of the diesel engine considered in the study. In the figure, the torsional vibrations calculated according to the optimized damping (c_{11})

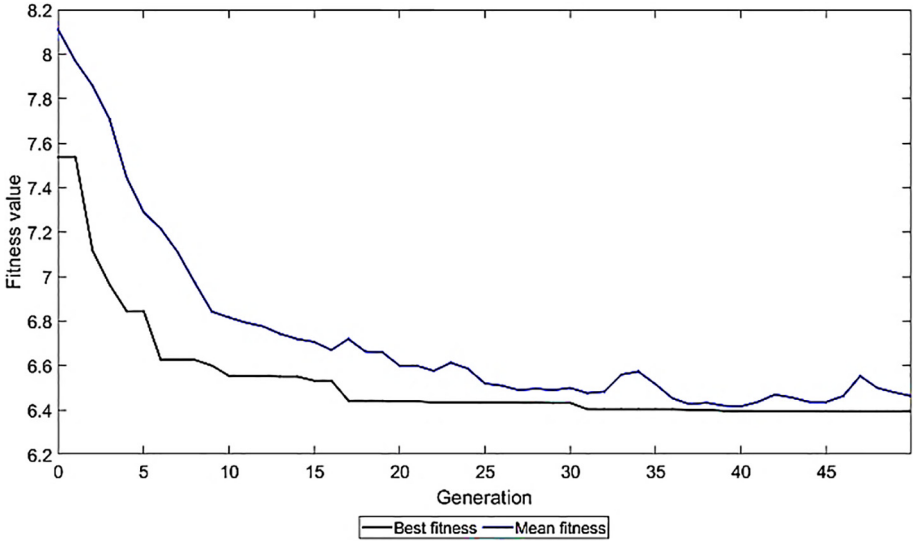

Fig 12. Best and mean fitness generation of the proposed GA optimization.

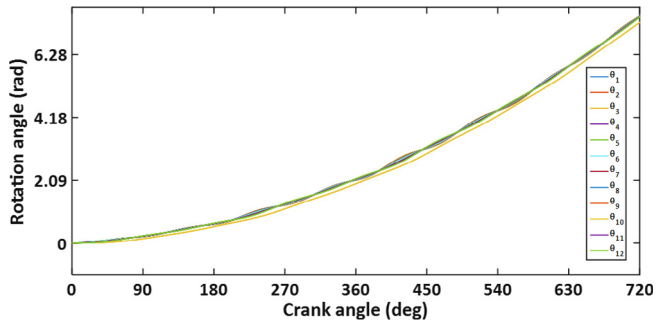

Fig 13. The result of the rotational angles of the lumped mass model as to crank angle.

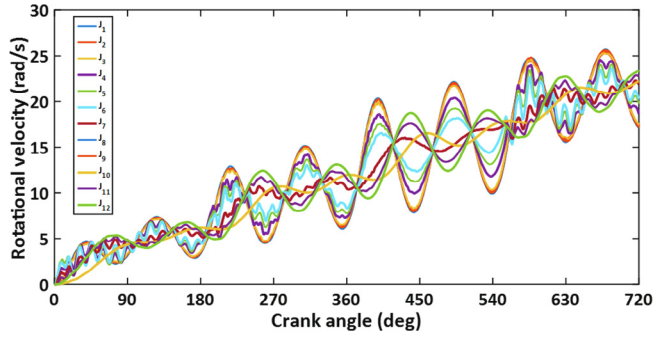

Fig 14. The result of the angular velocities of the lumped mass model as to crank angle.

and the stiffness coefficient (k_{11}) of the silicone fluid. The torsional vibrations are compared in case of optimized and non-optimized usage of DMRV-TVD as well as without using DMRV-TVD.

It is seen from the figure that the torsional vibration between 540 and 630 degrees peaks in the negative direction. By using the genetic algorithm method, the absolute value of all the torsional vibration values between 540 and 630 degrees are aimed to fit to zero. Also, the negative peak of the torsional vibration value is aimed to fit to zero with a higher coefficient. Table 2 gives the parameters for silicone oil materials and geometry constraints used in this study. As seen from the table that nine variables are used as optimization parameters. That are, four material property parameters for the stiffness coefficient (k_{11}), four parameters related to the damping coefficient (c_{11}) of the silicone fluid and one parameter that is related to the amount of the silicon fluid which is common for k_{11} and c_{11}.

In Table 2, the stiffness (k_{11}) and damping (c_{11}) coefficients of the silicone fluid are optimized with the parameters obtained from Eqs. (6) and (7) to eliminate the torsional vibrations from the crankshaft and pulley (J_{10}). The material properties of a silicone fluid with a viscosity of 0.2 m^2/s are used as non-optimized values. The material parameters in the minimum and maximum value range are determined according to the material properties in the 0.1 m^2/s and 1 m^2/s viscosity range. GA optimization is realized through Matlab software and it is revealed that the rigidity and damping coefficients should be reduced to a certain value to reach the optimum vibration damping capability. The inertial mass (J_{12}) moving through the silicone fluid with reduced stiffness and damping coefficients will rotate against a lower resistance after optimization. The non-optimized and the optimized values of k_{11} and c_{11} in this study are given in Table 3. The comparative results show that the developed hybrid design of optimized DMRV-TVD reduced the torsional vibrations by 50.17% when compared to the non-optimized DMRV-TVD. A periodogram graphic shown in Fig. 16 is created to estimate the spectral density before and after optimizations according to damping ($c11$) and the stiffness coefficient ($k11$) of the silicone fluid.

The torsional vibration effect of the optimized damping coefficient (c_{11}) and the stiffness coefficient (k_{11}) of the silicone fluid of the DMRV-TVD on the pulley (J_{10}) is shown in Fig. 17. As a result of the response of the pulley, the optimized silicone fluid of the DMRV-TVD reduced the torsional vibration by 79.65% when compared to the non-optimized DMRV-TVD.

The achievements in similar studies are given as follows for comparison although they do not have the same engines and TVDs. Tamkhade et al [43] have produced four TVD models and prototypes using silicon fluids of different amounts and viscosities. Torsional vibration amplitudes have been compared experimentally and theoretically. In the reported work, a reduction in torsional vibrations of approximately 67% is achieved for sample four by using a lower amount of low viscosity silicone fluid than the others. However, due to the high temperature that emerged in this model, it ensured that sample three, which is used in the same viscosity in a larger amount, is selected as the optimum TVD. In sample three, torsional vibrations are reduced by about 60%. According to the excitation torque map, implications were made about what

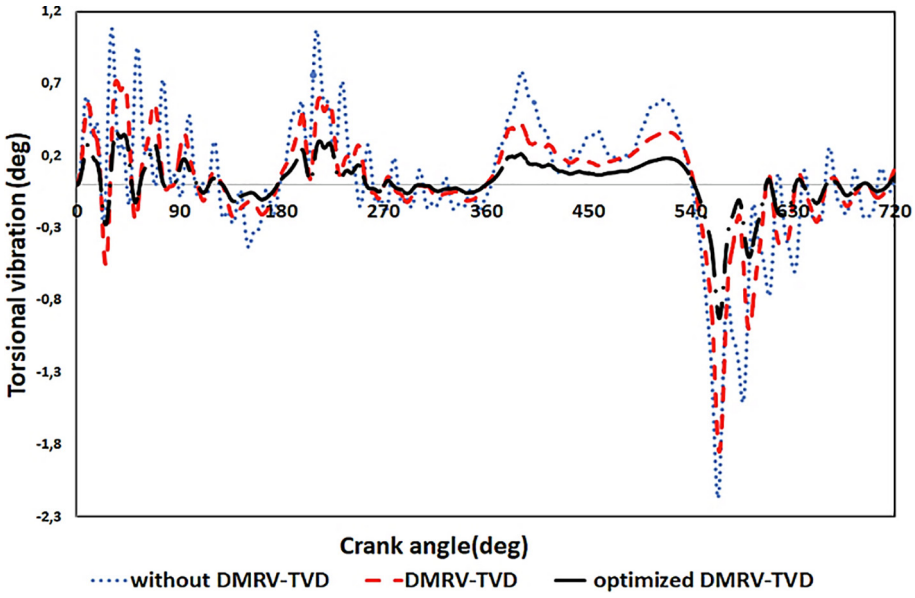

Fig 15. The effect of the optimized DMRV-TVD on the torsional vibrations of the on crankshaft end (J_7) according to damping (c_{11}) and the stiffness coefficient (k_{11}) of the silicone fluid.

Table 2
Silicone oil material, geometry constraints and optimized values.

	G_k	B_k	a_k	a_{k1}	G_c	B_c	a_c	a_{c1}	S
Non-optimized value	105×10^{-4}	3511	2.15	451	1.36	2405	1.55	351	5
Min. value	21×10^{-4}	3630	1.452	439	0.75	2342	1.49	293	2
Max value	8.61×10^{-3}	4297	3.2	614	6.84	2974	2.09	555	10
Optimized value	64×10^{-4}	3700	1.7	453	0.75	2342	1.49	544	2.16

Table 3
Silicone oil material optimized values and analysis elapsed time.

Non-Optimized c_{11}	160	Optimized c_{11}	4.4
Non-Optimized k_{11}	1.81×10^4	Optimized k_{11}	1403
Elapsed Time (s)	2809		

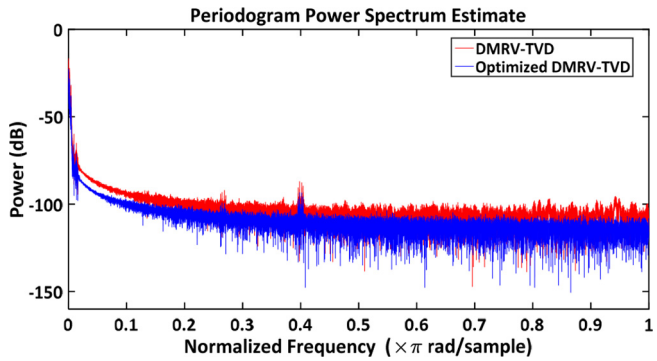

Fig 16. The estimation of the spectral density of before and after optimizations according to damping (c_{11}) and the stiffness coefficient (k_{11}) of the silicone fluid.

kind of TVD design should be made. Torsional vibration dampers can be manufactured from containing rubber-dampers, viscous dampers, or both. Since the mechanical behaviors of rubber and silicone materials do not show a linear elastic, methods specific to the material models should be used in the calculation of stiffness and damping coefficients. In another literature work, a new model is developed for torsional vibration damper, a viscoelastic material and a torsion spring are designed as a couple by Píštěk et al. [9].

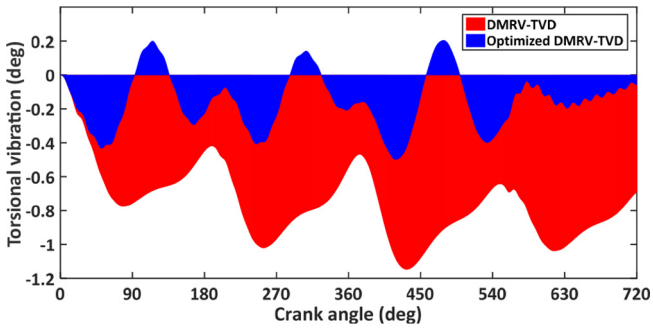

Fig 17. The effect of the optimized DMRV-TVD on the pulley (J_{10}) relative to before optimization on the torsional vibrations according to damping (c_{11}) and the stiffness coefficient (k_{11}) of the silicone fluid.

Since rubber dampers are very sensitive to temperature and silicon fluids have poor damping capabilities, this model has been developed in which silicon oil and torsion springs are used together. Approximately 60% more stable torque transfer is achieved compared to the model without TVD, and approximately 80% viscous damper In a study, using an internal combustion engine similar to the used in this article, the torsional vibrations of viscous and rubber TVD's are compared [1]. A novel hybrid design DMRV-TVD that combines rubber and viscous materials obtained in this study, give better results than the aforementioned study.

According to achieved optimized torsional vibration results in this study, stiffness and damping coefficient values are decreased using the GA optimization. It can be said that these values can be achieved by choosing a lower viscosity silicon fluid and reducing the amount of material. In the non-optimized silicon fluid parameters, the low rotation and the low angular velocity of the inertia

mass are realized, but with the new silicon fluid parameters, the inertia mass moves more freely in the silicon fluid and the effectiveness of the inertia mass on the torsional vibrations are increased. A much more robust motion of the crank shaft is obtained with the new parameters at the 2100 rpm of the most critical engine speed.

6. Conclusions

This paper is on the phenomenon of crankshaft torsional vibration in internal combustion engines (ICE). Especially in heavy-duty diesel engines, torsional vibration dampers (TVD) with rubber dampers or viscous dampers have been used to control the torsional vibrations occurring in the cranktrain system. In this research a hybrid damping approach is proposed for a better damping capacity. That is, a double mass rubber and viscous torsional vibration damper (DMRV-TVD) are used and optimized by genetic algorithm (GA) to find a better damping performance on cranktrain of an ICE. The obtained results showed that the novel hybrid design optimized DMRV-TVD reduced the torsional vibrations by 50.17% on crankshaft end and by 79.65% on pulley when compared to the non-optimized DMRV-TVD. The proposed approaches used to find stiffness and damping coefficients reported in this study can be employed for multi degree of freedom vibration systems.

In the future, it is planned to optimization of the rubber material using various powerful optimization methods such as genetic algorithm (GA), cuckoo search (CS), teaching–learning-based optimization (TLBO), the bees algorithm (BA) and Jaya algorithms, and the comparison of the proposed optimization methods will be realized to developed the torsional vibration damping effect of the DMRV-TVD.

Declaration of Competing Interest

The authors declare that they have no known competing financial interests or personal relationships that could have appeared to influence the work reported in this paper.

Appendix 1:. The extended state space model.

$$
\begin{bmatrix} \dot\theta_1 \\ \ddot\theta_1 \\ \dot\theta_2 \\ \ddot\theta_2 \\ \dot\theta_3 \\ \ddot\theta_3 \\ \dot\theta_4 \\ \ddot\theta_4 \\ \dot\theta_5 \\ \ddot\theta_5 \\ \dot\theta_6 \\ \ddot\theta_6 \\ \dot\theta_7 \\ \ddot\theta_7 \\ \dot\theta_8 \\ \ddot\theta_8 \\ \dot\theta_9 \\ \ddot\theta_9 \\ \dot\theta_{10} \\ \ddot\theta_{10} \\ \dot\theta_{11} \\ \ddot\theta_{11} \\ \dot\theta_{12} \\ \ddot\theta_{12} \end{bmatrix} =
\begin{bmatrix}
0 & 1 & 0 & 0 & 0 & 0 & 0 & 0 & 0 & 0 & 0 & 0 & 0 & 0 & 0 & 0 & 0 & 0 & 0 & 0 & 0 & 0 & 0 & 0 \\
-\frac{k_1}{J_1} & -\frac{c_1}{J_1} & \frac{k_1}{J_1} & \frac{c_1}{J_1} & 0 & 0 & 0 & 0 & 0 & 0 & 0 & 0 & 0 & 0 & 0 & 0 & 0 & 0 & 0 & 0 & 0 & 0 & 0 & 0 \\
0 & 0 & 0 & 1 & 0 & 0 & 0 & 0 & 0 & 0 & 0 & 0 & 0 & 0 & 0 & 0 & 0 & 0 & 0 & 0 & 0 & 0 & 0 & 0 \\
\frac{k_1}{J_2} & \frac{c_1}{J_2} & \frac{-(k_1+k_2)}{J_2} & \frac{-(c_1+c_2)}{J_2} & \frac{k_2}{J_2} & \frac{c_2}{J_2} & 0 & 0 & 0 & 0 & 0 & 0 & 0 & 0 & 0 & 0 & 0 & 0 & 0 & 0 & 0 & 0 & 0 & 0 \\
0 & 0 & 0 & 0 & 0 & 1 & 0 & 0 & 0 & 0 & 0 & 0 & 0 & 0 & 0 & 0 & 0 & 0 & 0 & 0 & 0 & 0 & 0 & 0 \\
0 & 0 & \frac{k_2}{J_3} & \frac{c_2}{J_3} & \frac{-(k_2+k_3)}{J_3} & \frac{-(c_2+c_3)}{J_3} & \frac{k_3}{J_3} & \frac{c_3}{J_3} & 0 & 0 & 0 & 0 & 0 & 0 & 0 & 0 & 0 & 0 & 0 & 0 & 0 & 0 & 0 & 0 \\
0 & 0 & 0 & 0 & 0 & 0 & 0 & 1 & 0 & 0 & 0 & 0 & 0 & 0 & 0 & 0 & 0 & 0 & 0 & 0 & 0 & 0 & 0 & 0 \\
0 & 0 & 0 & 0 & \frac{k_3}{J_4} & \frac{c_3}{J_4} & \frac{-(k_3+k_4)}{J_4} & \frac{-(c_3+c_4)}{J_4} & \frac{k_4}{J_4} & \frac{c_4}{J_4} & 0 & 0 & 0 & 0 & 0 & 0 & 0 & 0 & 0 & 0 & 0 & 0 & 0 & 0 \\
0 & 0 & 0 & 0 & 0 & 0 & 0 & 0 & 0 & 1 & 0 & 0 & 0 & 0 & 0 & 0 & 0 & 0 & 0 & 0 & 0 & 0 & 0 & 0 \\
0 & 0 & 0 & 0 & 0 & 0 & \frac{k_4}{J_5} & \frac{c_4}{J_5} & \frac{-(k_4+k_5)}{J_5} & \frac{-(c_4+c_5)}{J_5} & \frac{k_5}{J_5} & \frac{c_5}{J_5} & 0 & 0 & 0 & 0 & 0 & 0 & 0 & 0 & 0 & 0 & 0 & 0 \\
0 & 0 & 0 & 0 & 0 & 0 & 0 & 0 & 0 & 0 & 0 & 1 & 0 & 0 & 0 & 0 & 0 & 0 & 0 & 0 & 0 & 0 & 0 & 0 \\
0 & 0 & 0 & 0 & 0 & 0 & 0 & 0 & \frac{k_5}{J_6} & \frac{c_5}{6} & \frac{-(k_5+k_6)}{J_6} & \frac{-(c_5+c_6)}{J_6} & \frac{k_6}{J_6} & \frac{c_6}{J_6} & 0 & 0 & 0 & 0 & 0 & 0 & 0 & 0 & 0 & 0 \\
0 & 0 & 0 & 0 & 0 & 0 & 0 & 0 & 0 & 0 & 0 & 0 & 0 & 1 & 0 & 0 & 0 & 0 & 0 & 0 & 0 & 0 & 0 & 0 \\
0 & 0 & 0 & 0 & 0 & 0 & 0 & 0 & 0 & 0 & \frac{k_6}{J_7} & \frac{c_6}{J_7} & \frac{-(k_6+k_7)}{J_7} & \frac{-(c_6+c_7)}{J_7} & \frac{k_7}{J_7} & \frac{c_7}{J_7} & 0 & 0 & 0 & 0 & 0 & 0 & 0 & 0 \\
0 & 0 & 0 & 0 & 0 & 0 & 0 & 0 & 0 & 0 & 0 & 0 & 0 & 0 & 0 & 1 & 0 & 0 & 0 & 0 & 0 & 0 & 0 & 0 \\
0 & 0 & 0 & 0 & 0 & 0 & 0 & 0 & 0 & 0 & 0 & 0 & \frac{k_7}{J_8} & \frac{c_7}{J_8} & \frac{-(k_7+k_8+k_{10}+k_{11})}{J_8} & \frac{-(c_7+c_8+c_{10}+c_{11})}{J_8} & \frac{k_8}{J_8} & \frac{c_8}{J_8} & 0 & 0 & \frac{k_{10}}{J_8} & \frac{c_{10}}{J_8} & \frac{k_{11}}{J_8} & \frac{c_{11}}{J_8} \\
0 & 0 & 0 & 0 & 0 & 0 & 0 & 0 & 0 & 0 & 0 & 0 & 0 & 0 & 0 & 0 & 0 & 1 & 0 & 0 & 0 & 0 & 0 & 0 \\
0 & 0 & 0 & 0 & 0 & 0 & 0 & 0 & 0 & 0 & 0 & 0 & 0 & 0 & \frac{k_8}{J_9} & \frac{c_8}{J_9} & \frac{-(k_8+k_9)}{J_9} & \frac{-(c_8+c_9)}{J_9} & \frac{k_9}{J_9} & \frac{c_9}{J_9} & 0 & 0 & 0 & 0 \\
0 & 0 & 0 & 0 & 0 & 0 & 0 & 0 & 0 & 0 & 0 & 0 & 0 & 0 & 0 & 0 & 0 & 0 & 0 & 1 & 0 & 0 & 0 & 0 \\
0 & 0 & 0 & 0 & 0 & 0 & 0 & 0 & 0 & 0 & 0 & 0 & 0 & 0 & 0 & 0 & \frac{k_9}{J_{10}} & \frac{c_9}{J_{10}} & -\frac{k_9}{J_{10}} & -\frac{c_9}{J_{10}} & 0 & 0 & 0 & 0 \\
0 & 0 & 0 & 0 & 0 & 0 & 0 & 0 & 0 & 0 & 0 & 0 & 0 & 0 & 0 & 0 & 0 & 0 & 0 & 0 & 0 & 1 & 0 & 0 \\
0 & 0 & 0 & 0 & 0 & 0 & 0 & 0 & 0 & 0 & 0 & 0 & 0 & 0 & \frac{k_{10}}{J_{11}} & \frac{c_{10}}{J_{11}} & 0 & 0 & 0 & 0 & -\frac{k_{10}}{J_{11}} & -\frac{c_{10}}{J_{11}} & 0 & 0 \\
0 & 0 & 0 & 0 & 0 & 0 & 0 & 0 & 0 & 0 & 0 & 0 & 0 & 0 & 0 & 0 & 0 & 0 & 0 & 0 & 0 & 0 & 0 & 1 \\
0 & 0 & 0 & 0 & 0 & 0 & 0 & 0 & 0 & 0 & 0 & 0 & 0 & 0 & \frac{k_{11}}{J_{12}} & \frac{c_{11}}{J_{12}} & 0 & 0 & 0 & 0 & 0 & 0 & -\frac{k_{11}}{J_{12}} & -\frac{c_{11}}{J_{12}}
\end{bmatrix}
\begin{bmatrix} \theta_1 \\ \dot\theta_1 \\ \theta_2 \\ \dot\theta_2 \\ \theta_3 \\ \dot\theta_3 \\ \theta_4 \\ \dot\theta_4 \\ \theta_5 \\ \dot\theta_5 \\ \theta_6 \\ \dot\theta_6 \\ \theta_7 \\ \dot\theta_7 \\ \theta_8 \\ \dot\theta_8 \\ \theta_9 \\ \dot\theta_9 \\ \theta_{10} \\ \dot\theta_{10} \\ \theta_{11} \\ \dot\theta_{11} \\ \theta_{12} \\ \dot\theta_{12} \end{bmatrix} +
\begin{bmatrix}
0 & 0 & 0 & 0 \\
0 & 0 & 0 & 0 \\
0 & 0 & 0 & 0 \\
0 & 0 & 0 & 0 \\
0 & 0 & 0 & 0 \\
\frac{1}{J_3} & 0 & 0 & 0 \\
0 & 0 & 0 & 0 \\
0 & \frac{1}{J_4} & 0 & 0 \\
0 & 0 & 0 & 0 \\
0 & 0 & \frac{1}{J_5} & 0 \\
0 & 0 & 0 & 0 \\
0 & 0 & 0 & \frac{1}{J_6} \\
0 & 0 & 0 & 0 \\
0 & 0 & 0 & 0 \\
0 & 0 & 0 & 0 \\
0 & 0 & 0 & 0 \\
0 & 0 & 0 & 0 \\
0 & 0 & 0 & 0 \\
0 & 0 & 0 & 0 \\
0 & 0 & 0 & 0 \\
0 & 0 & 0 & 0 \\
0 & 0 & 0 & 0 \\
0 & 0 & 0 & 0 \\
0 & 0 & 0 & 0
\end{bmatrix}
\begin{bmatrix} T_1 \\ T_2 \\ T_3 \\ T_4 \end{bmatrix}
$$

$$
\begin{bmatrix} \theta_1 \\ \theta_2 \\ \theta_3 \\ \theta_4 \\ \theta_5 \\ \theta_6 \\ \theta_7 \\ \theta_8 \\ \theta_9 \\ \theta_{10} \\ \theta_{11} \\ \theta_{12} \end{bmatrix} =
\begin{bmatrix}
1 & 0 & 0 & 0 & 0 & 0 & 0 & 0 & 0 & 0 & 0 & 0 & 0 & 0 & 0 & 0 & 0 & 0 & 0 & 0 & 0 & 0 & 0 & 0 \\
0 & 0 & 1 & 0 & 0 & 0 & 0 & 0 & 0 & 0 & 0 & 0 & 0 & 0 & 0 & 0 & 0 & 0 & 0 & 0 & 0 & 0 & 0 & 0 \\
0 & 0 & 0 & 0 & 1 & 0 & 0 & 0 & 0 & 0 & 0 & 0 & 0 & 0 & 0 & 0 & 0 & 0 & 0 & 0 & 0 & 0 & 0 & 0 \\
0 & 0 & 0 & 0 & 0 & 0 & 1 & 0 & 0 & 0 & 0 & 0 & 0 & 0 & 0 & 0 & 0 & 0 & 0 & 0 & 0 & 0 & 0 & 0 \\
0 & 0 & 0 & 0 & 0 & 0 & 0 & 0 & 1 & 0 & 0 & 0 & 0 & 0 & 0 & 0 & 0 & 0 & 0 & 0 & 0 & 0 & 0 & 0 \\
0 & 0 & 0 & 0 & 0 & 0 & 0 & 0 & 0 & 0 & 1 & 0 & 0 & 0 & 0 & 0 & 0 & 0 & 0 & 0 & 0 & 0 & 0 & 0 \\
0 & 0 & 0 & 0 & 0 & 0 & 0 & 0 & 0 & 0 & 0 & 0 & 1 & 0 & 0 & 0 & 0 & 0 & 0 & 0 & 0 & 0 & 0 & 0 \\
0 & 0 & 0 & 0 & 0 & 0 & 0 & 0 & 0 & 0 & 0 & 0 & 0 & 0 & 1 & 0 & 0 & 0 & 0 & 0 & 0 & 0 & 0 & 0 \\
0 & 0 & 0 & 0 & 0 & 0 & 0 & 0 & 0 & 0 & 0 & 0 & 0 & 0 & 0 & 0 & 1 & 0 & 0 & 0 & 0 & 0 & 0 & 0 \\
0 & 0 & 0 & 0 & 0 & 0 & 0 & 0 & 0 & 0 & 0 & 0 & 0 & 0 & 0 & 0 & 0 & 0 & 1 & 0 & 0 & 0 & 0 & 0 \\
0 & 0 & 0 & 0 & 0 & 0 & 0 & 0 & 0 & 0 & 0 & 0 & 0 & 0 & 0 & 0 & 0 & 0 & 0 & 0 & 1 & 0 & 0 & 0 \\
0 & 0 & 0 & 0 & 0 & 0 & 0 & 0 & 0 & 0 & 0 & 0 & 0 & 0 & 0 & 0 & 0 & 0 & 0 & 0 & 0 & 0 & 1 & 0
\end{bmatrix}
\begin{bmatrix} \theta_1 \\ \dot\theta_1 \\ \theta_2 \\ \dot\theta_2 \\ \theta_3 \\ \dot\theta_3 \\ \theta_4 \\ \dot\theta_4 \\ \theta_5 \\ \dot\theta_5 \\ \theta_6 \\ \dot\theta_6 \\ \theta_7 \\ \dot\theta_7 \\ \theta_8 \\ \dot\theta_8 \\ \theta_9 \\ \dot\theta_9 \\ \theta_{10} \\ \dot\theta_{10} \\ \theta_{11} \\ \dot\theta_{11} \\ \theta_{12} \\ \dot\theta_{12} \end{bmatrix} +
\begin{bmatrix}
0 & 0 & 0 & 0 \\
0 & 0 & 0 & 0 \\
0 & 0 & 0 & 0 \\
0 & 0 & 0 & 0 \\
0 & 0 & 0 & 0 \\
0 & 0 & 0 & 0 \\
0 & 0 & 0 & 0 \\
0 & 0 & 0 & 0 \\
0 & 0 & 0 & 0 \\
0 & 0 & 0 & 0 \\
0 & 0 & 0 & 0 \\
0 & 0 & 0 & 0
\end{bmatrix}
\begin{bmatrix} T_1 \\ T_2 \\ T_3 \\ T_4 \end{bmatrix}
$$

Appendix 2:. Viscous material's constants.

Viscosity (m^2/s)	0.1	0.14	0.2
$G_{01}\left(\frac{N}{m^2}\right)$	21e-4	24e-4	105e-4
$G_{02}\left(\frac{N}{m^2}\right)$	0.75	1.04	1.36
$B_{01}(K)$	3630	3821	3511
$B_{02}(K)$	2342	2373	2405
$a_{01}(-)$	2.28	2.37	2.15
$a_{01}(-)$	1.49	1.51	1.55
$a_{11}(K)$	439	501	451
$a_{12}(K)$	293	319	351

Appendix 3:. Notation.

J	degree of freedom (–)	l	length (m)
C	total damping matrix (Nms/rad)	M	inertia matrix (kgm^2)
A	state matrix (–)	M (α)	torque (Nm)
a_p	piston acceleration (m^2/s)	m_p	piston mass (kg)
B	state matrix (–)	n	the engine speed (s^{-1})
c	damping coeffcient (Nms/rad)	P	cylinder pressure (bar)
C	state matrix (–)	r	crank radius (m)
C_r	relative damping matrix (Nms/rad)	S	clearance factor(m^3),
D	state matrix (–)	T	torque (Nm)
d	loss factor (–)	T	absolute mean temperature (K)
D	bore diameter (m)	*U*	input (–)
D_i	outer radius (m)	V	eigenvector (m)
D_o	inner radius (m)	*X*	state variable (–)
F_i	oscillating inertial force (N)	*Y*	output (–)
F_p	gas pressure force (N)	β	crankshaft angle (rad)
F_T	resulting tangential force (N)	θ	torsional vibration amplitudes (rad)
G_c	dynamic shear modulus (MPa)	λ	eigenvalue (Hz)
G_k	dynamic shear modulus (MPa)	λ	connecting rod length (m)
G_r	dynamic shear modulus (MPa)	χ	loss number (–)
j	the order number (–)	ω	crankshaft angular velocity (rad/s)
k	stiffness coeffcient (Nm/rad)	ω_n	system natural frequency (rad/s)
K_t	torsional stiffness matrix (Nm/rad)		

References

[1] A.S. Mendes, P.S. Meirelles, D.E. Zampieri, Analysis of torsional vibration in internal combustion engines: Modelling and experimental validation, Proc. IMechE 222 (2) (2008) 155–178, https://doi.org/10.1243/14644193JMBD126.

[2] P. Horváth, J. Égert, Dynamic analysis of a one-cylinder engine crankshaft, Acta Tech. Jaurinensis. 8 (2015) 280, https://doi.org/10.14513/actatechjaur.v8.n4.379.

[3] M. Cavalli, G. Lavacchielli, R. Tonelli, G. Nicoletto, E. Riva, Comparison of analytical and multibody dynamic approaches in the study of a V6 engine piston, Proc. Inst. Mech. Eng., Part K: J. Multi-body Dyn. 231 (3) (2017) 420–438, https://doi.org/10.1177/1464419317705988.

[4] K. Janssens, L. Britte, Comparison of torsional vibration measurement techniques, in: Proc. ISMA2012-USD2012 (2012) 1447–1462. https://doi.org/10.1007/978-3-642-39348-8_39.

[5] V. Píštek, D. Svída, Advanced Computational Models of Elastomer, Perner's Contacts. X (2015) 43–52.

[6] S. Ni, Y. Guo, W. Li, D. Wang, Z. Shuai, D. Yu, Effect of advanced injection angle on diesel engine shaft torsional vibration, Int. J. Engine Res. (2020) 1–8, https://doi.org/10.1177/1468087419895932.

[7] C.A.F. Silva, L. Manin, R.G. Rinaldi, E. Besnier, D. Remond, Dynamics of Torsional Vibration Damper (TVD) pulley, implementation of a rubber elastomeric behavior, simulations and experiments, Mech. Mach. Theory 142 (2019), https://doi.org/10.1016/j.mechmachtheory.2019.103583. 103583.

[8] L. Sun, F. Luo, T. Shang, H. Chen, A. Moro, Research on torsional vibration reduction of crankshaft in off-road diesel engine by simulation and experiment, J. Vibroeng. 20 (1) (2018) 345–357, https://doi.org/10.21595/jve.2017.18318.

[9] M. Píštěk, V. Kučera, P. Svída, D. Beran, A torsional vibration damper based on a serial viscoelastic coupling of its seismic mass, in: Vibroengineering Procedia, JVE International, 2017, pp. 56–60, https://doi.org/10.21595/vp.2017.19503.

[10] K. Sentyakov, J. Peterka, V. Smirnov, P. Bozek, V. Sviatskii, Modeling of boring mandrel working process with vibration damper, Materials (Basel) 13 (2020) 1–13, https://doi.org/10.3390/MA13081931.

[11] X. Tan, L. Hua, C. Lu, C. Yang, Y. Wang, S. Wang, A new method for optimizing the parameters of torsional vibration dampers, J. Vibroeng. 19 (6) (2017) 4155–4171, https://doi.org/10.21595/jve.2017.18579.

[12] X. Storm, J. Hyvonen, H.J. Salminen, R. Virrankoski, S. Niemi, Crank Shaft Torsional Vibration Analysis on the perspective of Improving the Crank Angle Measurement Accuracy for Closed-loop Combustion Control in ICES, in: SAE Tech. Pap. 2018-April (2018) 1–13. https://doi.org/10.4271/2018-01-1161.

[13] Y. Huang, S. Yang, F. Zhang, C. Zhao, Q. Ling, H. Wang, Non-linear torsional vibration characteristics of an internal combustion engine crankshaft assembly, Chin. J. Mech. Eng. 25 (4) (2012) 797–808, https://doi.org/10.3901/CJME.2012.04.797.

[14] P.S. Meirelles, D.E. Zampieri, A.S. Mendes, Mathematical Model for Torsional Vibration Analysis in Internal Combustion Engines AMURE AUV and LMA View project AAS Consulting-Advanced CAE Simulations View project (2007). <https://www.researchgate.net/publication/327510635>.

[15] H. Zhu, W. Chen, R. Zhu, J. Gao, M. Liao, Study on the dynamic characteristics of a rotor bearing system with damping rings subjected to base vibration, J. Vib. Eng. Technol. 8 (1) (2020) 121–132, https://doi.org/10.1007/s42417-019-00082-8.

[16] R. Talebitooti, M. Morovati, Study on TVD parameters sensitivity of a crankshaft using multiple scale and state space method considering quadratic and cubic non-linearities, Lat. Am. j. solids struct. 11 (14) (2014) 2672–2695, https://doi.org/10.1590/S1679-78252014001400007.

[17] S. Kim, H. Shin, S. Rhim, K.Y. Rhee, Calibration of hyperelastic and hyperfoam constitutive models for an indentation event of rigid polyurethane foam, Compos. B Eng. 163 (2019) 297–302, https://doi.org/10.1016/j.compositesb:2018.11.045.

[18] R.G. Desavale, A.M. Patil, Theoretical and experimental analysis of torsional and bending effect on four cylinders engine crankshafts by using finite element approach, Int. J. Eng. Res. 2 (2013) 379–385.

[19] J. Quiroga, O. Bohórquez, J. Ardila, V. Bonilla, N. Cortés, E. Martínez, Torsional natural frequencies by Holzer method, J. Phys. Conf. Ser. 1160 (2019) 012008, https://doi.org/10.1088/1742-6596/1160/1/012008.

[20] J. Sheng, M. He, M. Yao, Simulation study on the performance of a rubber-type torsional vibration damper, DEStech Trans. Eng. Technol. Res. 3 (2018) 79–84, https://doi.org/10.12783/dtetr/amme2017/19486.

[21] V.C. Shahane, R.S. Pawar, Optimization of the crankshaft using finite element analysis approach, Automot. Engine Technol. 2 (2017) 1–23, https://doi.org/10.1007/s41104-016-0014-0.

[22] W. Mitianiec, K. Buczek, Torsional vibration analysis of crankshaft in heavy duty six cylinder inline engine, Czas. Tech. Mech. (2008) 193–207.

[23] A.D. Foltz, T.M. Wasfy, E. Ostergaard, I. Piraner, Multibody Dynamics Model of a Diesel Engine and Timing Gear Train with Experimental Validation (2016). <http://proceedings.asmedigitalcollection.asme.org/pdfaccess.ashx?url=/data/conferences/asmep/90984/>.

[24] L. Drápal, P. Novotný, Torsional vibration analysis of crank train with low friction losses, J. Vibroeng. 19 (2017) 5691–5701, https://doi.org/10.21595/jve.2017.17876.

[25] E. Armentani, F. Caputo, L. Esposito, V. Giannella, R. Citarella, Multibody simulation for the vibration analysis of a turbocharged diesel engine, Appl. Sci. 8 (2018), https://doi.org/10.3390/app8071192.

[26] H. Karimaei, M. Mehrgou, H.R. Chamani, Optimisation of torsional vibration system for a heavy-duty inline six-cylinder diesel engine, Proc. Inst. Mech. Eng. Part K J. Multi-Body Dyn. 233 (2019) 642–656, https://doi.org/10.1177/1464419319826744.

[27] K.S.K. Wakabayashi, Y. Honda, T. Kodama, Torsional vibration damping of diesel engine with rubber damper pulley, JSME Int J., Ser. C 38 (1995) 670–678.

http://www.mendeley.com/research/geology-volcanic-history-eruptive-style-yakedake-volcano-group-central-japan/.
[28] S.S. Ramdasi, N. V. Marathe, Predictive-Cum-Experimental Analysis of Torsional/Bending and Crankcase Vibrations and Design of Optimum Tuned Damper, in: SAE Tech. Pap. 2004-Janua (2004). https://doi.org/10.4271/2004-28-0022.
[29] S.G. Villalva, M.L. Bittencourt, P.R. Zampieri, Methodology for automotive crankshaft design using analytical and flexible models, in: SAE Tech. Pap. 13 (2013). https://doi.org/10.4271/2013-36-0590.
[30] V. Píštek, P. Kucera, O. Nozhenko, K. Kravchenko, D. Svída, An unconventional rubber torsional vibration damper with two degrees of freedom, Vibroeng. Procedia 13 (2017) 136–141, https://doi.org/10.21595/vp.2017.19042.
[31] T. Kodama, Y. Honda, A study on the modeling and dynamic characteristics of the viscous damper silicone fluid by using vibration control of engine crankshaft system, Int. J. Mech. Eng. Robot. Res. 7 (2018) 273–278, https://doi.org/10.18178/ijmerr.7.3.273-278.
[32] S.K. Chen, T. Chang, Crankshaft torsional and damping simulation-An update and correlation with test results, in: SAE Tech. Pap. (1986). https://doi.org/10.4271/861226.
[33] I. Filipović, D. Bibić, A. Milašinović, A. Blažević, A. Pecar, Preliminary selection of basic parameters of different torsional vibration dampers intended for use in Medium Speed Diesel Engines, Trans. Famena 36 (2012) 79–88.
[34] I. Filipović, The parameter determination of the crankshaft dynamical model određivanje parametara dinamičkog modela kolenastog vratila (2011).
[35] M. Desbazeille, R.B. Randall, F. Guillet, M. El Badaoui, C. Hoisnard, Model-based diagnosis of large diesel engines based on angular speed variations of the crankshaft, Mech. Syst. Signal Process. 24 (2010) 1529–1541, https://doi.org/10.1016/j.ymssp.2009.12.004.
[36] P.D. Shah, P.K.K. Bhabhor, Finite element approach for study of torsional and bending effect on four cylinder engine crankshafts, Int. J. Thesis Proj. Diss. 2 (2014) 22–34.
[37] E.J. Nestrorides, Handbook on Torsional Vibration, British Internal Combustion Engine Research Association (B.I.C.E.R.A), Cambridge, 1958.
[38] H. Hafner, K.E. Maass, Theorie der triebwerk- sschwingungen der verbrennungskraftmaschine, Springer-Verlag, Wien, Berlin, 1984.
[39] H. Hafner, K.E. Maass, Torsionsschingungen in der Verbrennungs-kraftmaschine, Springer, 1985.
[40] Y. Gorash, T. Comlekci, R. Hamilton, CAE-Based application for identification and verification of hyperelastic parameters, Proc. Inst. Mech. Eng. Part L J. Mater. Des. Appl. 231 (2017) 611–626, https://doi.org/10.1177/1464420715604004.
[41] P.J. Carrato, C.C. Fu, Modal analysis techniques for torsional vibration of diesel crankshafts, in: SAE Tech. Pap. 95 (1986) 955–963. https://doi.org/10.4271/861225.
[42] Ü. Önen, A. Çakan, İ. İLhan, Performance comparison of optimization algorithms in LQR controller design for a nonlinear system, Turkish J. Electr. Eng. Comput. Sci. (2019), https://doi.org/10.3906/elk-1808-51.
[43] H.S. Tamkhade, G.S. Kondhalkar, Design and Development of Viscous Torsional Vibration Damper for Inline Six Cylinder Engine, PG-coordinator (n.d.).